lens and operated at 120 keV. A video system and a 30-μm condenser aperture were used during TEM examination to minimize beam damage, which can be significant for phases of SiO_2. Crucial to this work was the development of rapid data acquisition techniques to discriminate between amorphous material that was present in the sample and material that was caused by electron-beam damage. Further details that concern experimental techniques will be presented elsewhere [K. J. Kingma *et al.*, in preparation]. An ion mill, operating at 6 kV and accelerating Ar^+ ions from an 18° angle, was used to ion-thin all single-crystal quartz foils.

14. Planar defects and amorphous lamellae are typically observed in only one orientation in individual grains of TEM powder mounts. However, two or more sets of planar features, each in different crystallographic orientations, have been observed in several grains. Because all defects may not be in a diffracting orientation (visible in the TEM), multiple sets within single grains may be the norm. Further statistical analysis of the distribution of orientations is in progress.
15. Detailed examination of the behavior of quartz at these pressures on the basis of in situ x-ray observations will be presented elsewhere [K. J. Kingma, R. J. Hemley, H. K. Mao, in preparation].
16. Q. Williams and R. Jeanloz, in (*9*); an alcohol-water medium was used in this study. Isotropic bands in a decompressed single crystal were observed by optical microscopy.
17. Because the structure of SiO_2 glass changes with pressure [C. Meade, R. J. Hemley, H. K. Mao, *Phys. Rev. Lett.* **69**, 1387 (1992)], we expect that the structure of the amorphous phase varies with different synthesis conditions.
18. The fracture strength of quartz at ambient conditions is about 4 GPa [M. S. Paterson, *Experimental Rock Deformation—The Brittle Field* (Springer-Verlag, New York, 1978), p. 30]. However, stress concentrations in localized areas such as fractures and crack tips may be much higher. Amorphous SiO_2 on a TEM scale has been found along fractures that were formed during indentation deformation experiments that tested the fracture toughness of natural quartz [C. C. Ferguson, G. E. Lloyd, R. J. Knipe, *Can. J. Earth Sci.* **24**, 544 (1987)]. Stress-induced amorphization has also resulted from room temperature indentation of silicon and germanium single crystals [D. R. Clarke, M. C. Kroll, P. D. Kirchner, R. F. Cook, B. J. Hockey, *Phys. Rev. Lett.* **60**, 2156 (1988)] and from mechanical scratching of silicon [K. Minowa and K. Sumino, *ibid.* **69**, 320 (1992)].
19. J. M. Christie and A. J. Ardell, *Geology* **2**, 405 (1974); L. N. Dell'Angelo, *Eos* **71**, 458 (1991).
20. Similarities between amorphous phases that are produced by diamond-cell compression and by shock impact of silicates are described in (*16*). Luminescence associated with extreme localized heating has been observed during shock of quartz single crystals [P. J. Brannon *et al.*, *J. Appl. Phys.* **54**, 6374 (1983)]. No such luminescence was observed during our static compression experiments.
21. Examining a large number of samples, H.-R. Wenk [*Geology* **6**, 507 (1978)] concluded that pseudotachylites are formed by cataclasis, not by melting. Further examples are reviewed by R. A. Yund, M. L. Blanpied, T. E. Tullis, and J. D. Weeks [*J. Geophys. Res.* **95**, 15589 (1990)]. We suggest that solid-state amorphization that is associated with deformation at relatively low temperatures may give rise to these features.
22. C. Meade and R. Jeanloz, *Science* **252**, 68 (1991).
23. The high solubility of amorphous phases may obscure their formation in the geologic record. Amorphization of geologic materials may also occur in subduction zone environments (*22*).
24. S. Morris, *Proc. R. Acad. London* **436**, 203 (1992); stresses at crystalline-amorphous interfaces may have compressional, shear, or even tensile components. Additionally, even in the presence of a hydrostatic medium the formation of multiple crystalline blocks will produce nonhydrostatic stress at the block interfaces, which will in turn drive the breakdown of the parent crystalline form.
25. C. Meade, R. Jeanloz, R. J. Hemley, in *High Pressure Research: Applications to Earth and Planetary Sciences*, Y. Syono and M. H. Manghnani, Eds. (Terra Scientific, Tokyo, and American Geophysical Union, Washington, DC, 1992), pp. 485–492.
26. It will be important to examine the behavior of quartz at still higher pressures. Additionally, the role of amorphization of a metastable high-pressure phase or phases upon decompression should also be examined [as in (*27*)].
27. R. J. Hemley, L. C. Chen, H. K. Mao, *Nature* **338**, 638 (1989).
28. B. Pluis, W. D. van der Gon, J. W. M. Frenken, J. F. van der Veen, *Phys. Rev. Lett.* **59**, 2678 (1987).
29. L. E. McNeil and M. Grimsditch, *ibid.* **68**, 83 (1992).
30. We thank Q. Williams, R. Jeanloz, A. J. Gratz, R. M. Hazen, and R. E. Cohen for helpful discussions and correspondence. Supported by National Science Foundation (NSF) grants EAR-8920239 and EAR-9117858 (R.J.H. and H.K.M.) and NSF grant EAR-8903630 (D.R.V.).

15 September 1992; accepted 23 December 1992

The Hydrolytic Water Molecule in Trypsin, Revealed by Time-Resolved Laue Crystallography

Paul T. Singer, Arne Smalås, Robert P. Carty, Walter F. Mangel, Robert M. Sweet*

Crystals of bovine trypsin were acylated at the reactive residue, serine 195, to form the transiently stable *p*-guanidinobenzoate. Hydrolysis of this species was triggered in the crystals by a jump in pH. The hydrolysis was monitored by three-dimensional Laue crystallography, resulting in three x-ray diffraction structures, all from the same crystal and each representing approximately 5 seconds of x-ray exposure. The structures were analyzed at a nominal resolution of 1.8 angstroms and were of sufficient quality to reproduce subtle features in the electron-density maps for each of the structures. Comparison of the structures before and after the pH jump reveals that a water molecule has positioned itself to attack the acyl group in the initial step of the hydrolysis of this transient intermediate.

The serine protease trypsin has been studied extensively for decades, but there are still gaps in our understanding of the mechanism of proteolysis by trypsin. Like all serine proteases, trypsin acts in a two-step process. First, nucleophilic attack on a peptide bond by a serine hydroxyl group leads to the breaking of the peptide and formation of an ester bond between the carboxyl group and the serine hydroxyl. The hydroxyl group is activated by a nearby histidine and a buried aspartate, which form the "catalytic triad" (*1*). This intermediate is subsequently hydrolyzed by a water molecule, regenerating the hydroxyl and releasing the second half of the cleaved protein. That this water molecule itself is activated by the catalytic triad, in a mechanism that mirrors the initial reaction, has always been assumed. In order to explore the hydrolysis of the ester intermediate, we have prepared a transiently stable species by reaction of the enzyme with *p*-nitrophenyl guanidinobenzoate to form *p*-guanidinobenzoyl (GB) trypsin (*2*, *3*). The form of the trypsin crystals that results has been investigated independently by Bartunik and co-workers (*4*). Release of the GB group can be controlled by pH; it is stable for days at low pH but only for hours at slightly above neutral pH. We used the Laue method of white-beam crystallography to collect x-ray diffraction data from a crystal of GB trypsin first at low pH, then immediately after the jump to high pH, and 90 min later at the higher pH. We addressed the following questions: Is the 1- to 2-min time resolution provided by the Laue measurement sufficient to trap a meaningful state along the catalytic pathway? Can the Laue method, which provides an inherently poor signal-to-noise ratio for diffraction data, reveal details as small as the motion of a side chain or water molecule? Can this model system provide insight into catalysis by serine proteases in general?

In a preliminary report of this work (*5*), we described the procedures used for the collection of Laue diffraction data. A single crystal of GB-substituted trypsin, measuring 1.0 mm by 0.4 mm by 0.4 mm, was mounted in a flow cell at pH 5.5. Between five and seven x-ray exposures were taken at beamline X26-C of the National Synchrotron Light Source. In order to counter damage of the specimen by the x-ray beam, the exposures were divided between two separated portions of the crystal, the spec-

P. T. Singer, Biology Department, Argonne National Laboratory, Argonne, IL 60439.
A. Smalås, Institute of Mathematical and Physical Science, University of Tromsø, N-9000 Tromsø, Norway.
R. P. Carty, Department of Biochemistry, State University of New York Health Science Center, Brooklyn, NY 11203.
W. F. Mangel and R. M. Sweet, Biology Department, Brookhaven National Laboratory, Upton, NY 11973.
*To whom correspondence should be addressed.

imen was rotated by 15° between exposures, and individual exposure times were 0.8 s. The pH of the elution buffer was raised to 8.5 after the first series of exposures, and, after a 3-min pause, the series of exposures was repeated on fresh portions of the crystal. Exposures were repeated 90 min later. Thus, diffraction data sufficient to determine three independent structures were measured from one crystal. The pH of the elution buffer was then lowered to 5.5 to quench the hydrolysis, the crystal was recovered, and the extent of GB acylation was assayed (*3*). The fraction of enzyme molecules that were acylated was 0.58. The Laue film data were reduced with the Daresbury suite of programs (*6*), yielding 13,100 reflections at the low pH point (designated hereafter as t_0), 18,600 at 3 min after the pH jump (t_3), and 16,800 at t_{90}.

The starting point for the refinement of the three structures was the 2.0 Å model of GB trypsin (*3*). Procedures for and results from the crystallographic refinement appear in Table 1. We used conventional positional and *B*-factor (Debye-Waller isotropic temperature factor) refinement plus simulated annealing refinement, which was supplemented by manual model building and visual inspection of the electron density maps. Occupancy refinement for the GB group was done to estimate the degree of acylation in each structure. This refinement was performed first with concomitant refinement of the group's *B* factors and then with the *B* factors for each of the three structures fixed to the value to which each had refined in the t_0 structure. Because *B* factors and occupancies are tightly coupled variables, this method allowed us to compare the GB occupancies among the three time-resolved structures.

Analysis of the water structure in the active-site region was handled with special care. Electron density peaks often appeared in the omit maps as possible water molecules but did not reappear after the atoms were included. This disappearance prompted us to repeat the process of successively calculating electron density maps with the active site water structure omitted. Only atoms that reappeared after further refinement are included in the final models. In the final steps of the refinements, only the water molecules that refined to temperature factors less than 50 Å^2 were included.

The quality of the electron density maps is high in general. The t_3 and t_{90} maps are better than the t_0 map, which probably reflects the quality and quantity of the

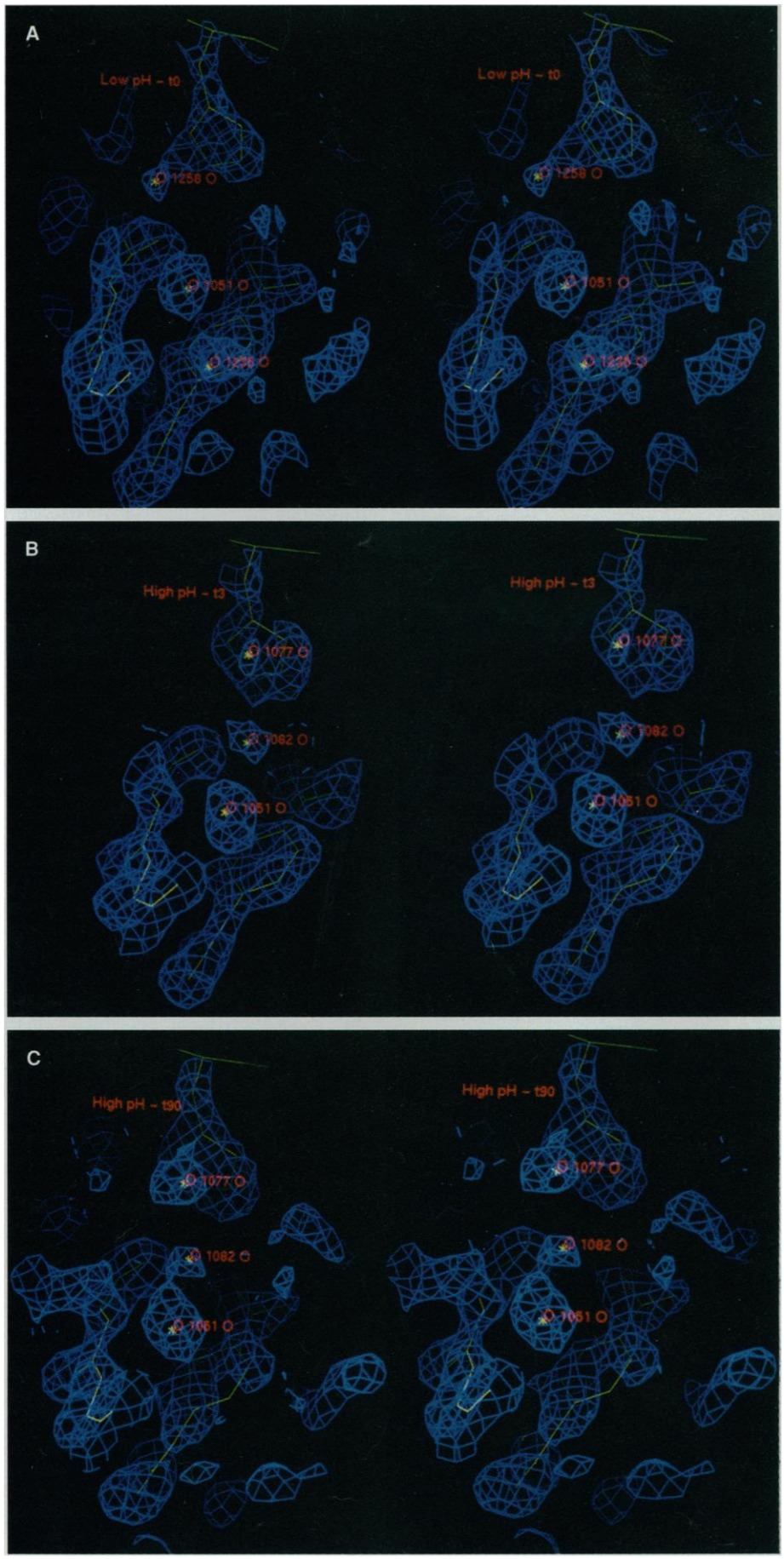

Fig. 1. Stereo images of electron density maps for the three GB-trypsin structures. The maps shown are from coefficients $|2F_o - F_c|$, phased with F_c, and contoured at 1.5σ. (**A**) t_0, (**B**) t_3, and (**C**) t_{90}.

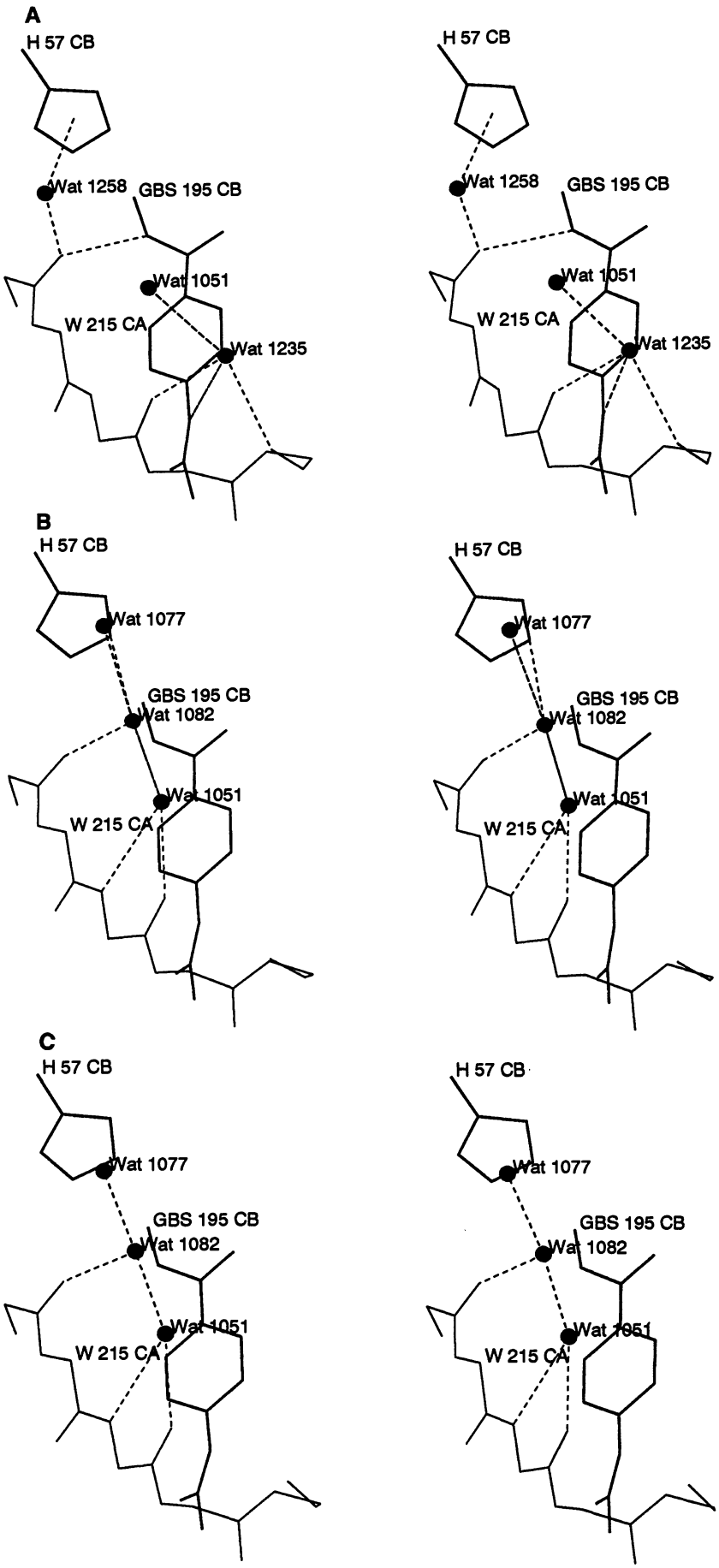

Fig. 2. Stereo images of close contacts among water molecules and the GB-trypsin molecule for the three structures: (**A**) t_0, (**B**) t_3, and (**C**) t_{90}. All contacts shown by dashed lines are less than 3.4 Å. GBS CB refers to the Cβ of the guanidinobenzoyl serine, and W CA is the Cα of the Trp.

intensity data. The final refinement parameters for t_3 and t_{90} are also better (Table 1). The protein core is well defined for all three structures with continuous electron density and, for example, distinct holes in the density corresponding to aromatic side chains. However, external loops are less well defined than expected for protein structures refined to this degree. The accuracies of the final models, estimated from Luzatti plots (*7*), are ≈0.2 Å.

Another assessment of the accuracy of the structures can be made from the coordinate differences between pairs of the three models (Table 2). Except perhaps for the fine differences this study is intended to discover, the models are fundamentally the same. The mean differences between backbone atoms are less than 0.2 Å. The GB-group statistics show that in the t_{90} structure this group is most different from the others, possibly because of the lower occupancy of this GB group. Surprisingly, when we consider all atoms, the t_0 and t_{90} structures are most similar. It is possible that the t_3 structure was disrupted by the pH jump in the flow cell but reannealed after 90 min at the higher pH. This disruption is mirrored in part in the mean *B* factor for the low pH structure, which is lower than for the two high pH structures; the apparent higher mobility of the high pH structures may result from the shock of the pH jump. Comparison of plots of the *B* factors against the amino acid sequence for the three structures does not reveal regions with clear differences in the *B*-factor profile.

The importance of the experiment is revealed in the time evolution of the electron-density maps (Fig. 1). The most dramatic feature of the t_3 map, representing the structure just after the pH jump, is the water molecule labeled 1082 (Wat^{1082}) that appears in a position to attack the scissile bond. The molecule appears again, slightly shifted, in the t_{90} map. The refined *B* factors for these atoms are 30 and 27 $Å^2$, respectively. The refined atomic models for all three structures appear in Fig. 2. An additional feature of the refined models is the gradual shifting of the His^{57} imidazole group away from the hydrolytic water molecule during the experiment (Fig. 3). This shift, a total of 0.6 Å, is significant compared to the limits of reliability of the refinement.

The reliability of Wat^{1082} in the t_3 structure, on which the argument depends, is

shown by the extent to which water molecules reappear in these Laue structures. Molecule 1051 (Fig. 1) is one example. Many others exist; 72 water molecules were found to be common to all three structures. Further evidence for the reliability of this interpretation comes from additional studies that compared high-resolution structures of benzamidine-inhibited trypsin under a variety of pH conditions, determined by both monochromatic and Laue techniques. In these additional studies, the active site water molecules, including several that appear in our structures, were absolutely reproducible (*8*).

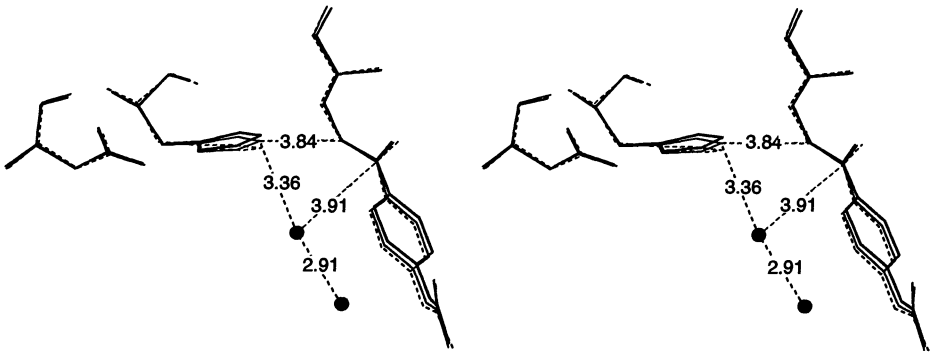

Fig. 3. Stereo images of contacts in the active-site region showing interatomic distances in angstroms for three structures: dashed, t_0; solid, t_3; and heavy line, t_{90}. Residue Asp^{102} is on the left, His^{57} in the middle, and guanidinobenzoyl Ser^{195} is to the right. The two water molecules shown are 1082 (upper dot) and 1051 (lower dot) from the t_3 structure (see Fig. 2B).

Table 1. Refinement results. Crystallographic refinement was performed with the computer program X-PLOR (*11*). The starting coordinates for the protein portion of the model were from a structure of GB trypsin derived from refinement with a 2.0 Å monochromatic data set (*3*). The starting solvent model consisted of 248 water molecules that had been identified during preliminary studies as existing in at least one of the three structures. All three Laue structures were refined with the same protocol and with this model for solvation. First, 40 cycles of positional refinement with the Powell CG (conjugate-gradient) minimizer, 20 cycles of *B*-factor refinement, and another 40 cycles of CG refinement were used for a preliminary fitting. We refined the structures further using the simulated annealing protocol. The structure was heated to 3000 K and cooled in increments of 25 K, after each of which 50 steps of molecular dynamics simulation were performed, each representing 0.5 fs. Subsequently, 120 cycles of CG refinement were performed before the resulting electron density maps were inspected [CHAIN program suite (*12*)] and manual model building was performed. The final models were obtained after adjustments according to a series of omit maps with either $|F_o - F_c|$ or $|2F_o - F_c|$ Fourier coefficients (F_o and F_c are the observed and calculated structure factors, respectively), followed by CG and *B*-factor refinements. The final water structures were determined by model building from a series of omit maps, which were prepared after 20 more cycles of CG refinement from which the water molecules were omitted.

Parameter	GB-trypsin structure		
	t_0	t_3	t_{90}
Reflections (fraction of possible)*	11,140 (0.47)	15,400 (0.68)	14,230 (0.60)
Water molecules†	161	158	143
Initial *R* value	0.269	0.254	0.257
Final *R* value	0.221	0.183	0.187
δ_{bond}(Å)/ δ_{angle}(degrees)‡	0.016/3.32	0.013/2.77	0.014/2.87
Mean *B* factor (Å^2)			
Protein	12.8	15.1	15.7
Water	24.3	32.7	30.8
Occupancy of GB	0.99	0.97	0.91
B factor of GB (Å^2)	7.5	12.2	17.8
Occupancy of GB with fixed *B* of 7.5 Å^2	0.99	0.74	0.64

*Reflections with $I > 4\sigma_I$ in the resolution range 5.0 to 1.8 Å were included. The fraction of possible is based on the theoretical number of reflections in that range. †The number of protein atoms, including the GB group, was 1642. ‡Root-mean-square discrepancies from ideal values.

Table 2. Root-mean-square differences in position (Å) of selected groups of atoms in the three time-resolved Laue structures of trypsin.

Structures	All protein atoms	Backbone atoms	Side chain atoms	Internal residues	External residues	GB group
t_0 t_3	0.37	0.19	0.51	0.23	0.44	0.13
t_0 t_{90}	0.22	0.17	0.27	0.20	0.24	0.24
t_3 t_{90}	0.32	0.14	0.46	0.17	0.39	0.21

Although the hydrolytic water molecule lies directly above the plane of the ester carboxyl group in a position optimal for nucleophilic attack, there is neither a hydrogen bond to His^{57} nor a van der Waals bond with the carbonyl carbon atom, which is too distant. Nonetheless, its appearance in the electron density maps at high pH gives information about the nature of the activation process. At low pH, the imidazole of His^{57} is doubtless protonated, and the group carries a positive charge. The distance from the His^{57} Nϵ2 atom to the GB group changes very little on deprotonation during the shift from t_0 to t_3 (Fig. 3). The change in charge of the His^{57} side chain alone must be sufficient to stabilize the incoming hydrolytic water molecule.

There is a subtle shift in solvent coordination between t_0 and t_3, (Fig. 2, A and B). At t_0, molecules 1051 and 1258 occlude the hydrolytic site. Molecule 1051 forms a strong hydrogen bond with the rigidly coordinated Wat^{1235}, and Wat^{1258} lies above the plane of the His^{57} ring, resulting in a dipole-quadrupole interaction. At t_3, Wat^{1082} appears in a previously unoccupied space, making loose contact with His^{57} and the carbonyl carbon of GB-Ser^{195} and forming strong hydrogen bonds with the carbonyl oxygen atom (O) of residue 214 and with Wat^{1051}. After moving several angstroms, Wat^{1258} becomes Wat^{1077}, and Wat^{1051} moves 0.6 Å down and in to form two hydrogen bonds with the trypsin backbone, displacing Wat^{1235} completely. With interactive model building, it is easy to simulate the approach of the hydrolytic water molecule to the GB-group carbonyl carbon atom. The hydrogen bond to the Ser^{214} O atom can be maintained as the approach is made and a hydrogen bond to His^{57} Nϵ2 atom is formed and tightened. Both of these hydrogen bonds increase the nucleophilicity of the water molecule.

A water molecule appears in these structures in a site equivalent to that seen by Henderson (*9*), that is, it is perched on the tip of the carbonyl oxygen atom of indoleacryloyl-α-chymotrypsin. Our results suggest that this water molecule is not hydrolytic. Others (*10*) have seen evidence that the Ser^{214} O can form a hydrogen bond with the α-NH_2 group of the acylating amino acid. This NH_2 group is chemically equivalent to the ortho-carbon atoms of the benzene ring of GB, so it is likely that it lies far enough

from the imidazole ring of His^{57} to allow entry of the hydrolytic water molecule.

We believe we have resolved the issues posed at the beginning. Because the course of hydrolysis is slow, the time resolution was sufficient to trap the hydrolytic water molecule. The Laue method, judiciously applied, revealed details as subtle as the rearrangement of water molecules. Finally, the GB-trypsin system provided firm structural evidence for a role played by water during ester hydrolysis that is similar to that played by the serine hydroxyl during amide cleavage. Further, the experiment defined the geometry of the incoming water molecule, His^{57}, and the GB group and suggests an approach route for this molecule as it attacks the carbonyl carbon atom, becoming more nucleophilic as its interaction with the catalytic His residue increases.

REFERENCES AND NOTES

1. D. M. Blow, J. J. Birktoft, B. S. Hartley, *Nature* **221**, 337 (1969).
2. T. Chase, Jr., and E. Shaw, *Biochem. Biophys. Res. Commun.* **29**, 508 (1967).
3. W. F. Mangel *et al.*, *Biochemistry* **29**, 8351 (1990); Brookhaven Protein Data Bank entry 1GBT.
4. H. D. Bartunik, L. J. Summers, H. H. Bartsch, *J. Mol. Biol.* **210**, 813 (1989).
5. P. T. Singer *et al.*, *Philos. Trans. R. Soc. London Ser. A* **340**, 285 (1992).
6. J. R. Helliwell *et al.*, *J. Appl. Crystallogr.* **22**, 483 (1989).
7. V. Luzatti, *Acta Crystallogr.* **5**, 802 (1952).
8. P. T. Singer *et al.*, in preparation.
9. R. J. Henderson, *J. Mol. Biol.* **54**, 341 (1970).
10. For example, R. M. Sweet *et al.*, *Biochemistry* **13**, 4212 (1974).
11. X-PLOR; A. Brünger, Polygen, Waltham, MA.
12. J. S. Sack, *J. Mol. Graphics* **6**, 24 (1988).

13. P.T.S. was supported by an Alexander Hollaender Fellowship during much of this work. We acknowledge support for this work by the Office of Health and Environmental Research of the U.S. Department of Energy and by the National Science Foundation.

9 July 1992; accepted 2 October 1992

Structure of the Regulatory Complex of *Escherichia coli* III^{Glc} with Glycerol Kinase

James H. Hurley,* H. Rick Faber, David Worthylake,† Norman D. Meadow, Saul Roseman, Donald W. Pettigrew, S. James Remington‡

The phosphocarrier protein III^{Glc} is an integral component of the bacterial phosphotransferase (PTS) system. Unphosphorylated III^{Glc} inhibits non-PTS carbohydrate transport systems by binding to diverse target proteins. The crystal structure at 2.6 Å resolution of one of the targets, glycerol kinase (GK), in complex with unphosphorylated III^{Glc}, glycerol, and adenosine diphosphate was determined. GK contains a region that is topologically identical to the adenosine triphosphate binding domains of hexokinase, the 70-kD heat shock cognate, and actin. III^{Glc} binds far from the catalytic site of GK, indicating that long-range conformational changes mediate the inhibition of GK by III^{Glc}. GK and III^{Glc} are bound by hydrophobic and electrostatic interactions, with only one hydrogen bond involving an uncharged group. The phosphorylation site of III^{Glc}, His^{90}, is buried in a hydrophobic environment formed by the active site region of III^{Glc} and a 3_{10} helix of GK, suggesting that phosphorylation prevents III^{Glc} binding to GK by directly disrupting protein-protein interactions.

In *Escherichia coli*, the phosphoenolpyruvate:glycose phosphotransferase system (PTS) functions both as a transport pathway for its sugar substrates and as a negative regulator of the transport of several energy sources that are not PTS substrates (*1*). The regulatory state of the cell is determined by the state of phosphorylation of III^{Glc}, a PTS component specific for the uptake and phosphorylation of glucose. In the presence of PTS sugars, unphosphorylated III^{Glc} binds and inhibits permeases and other enzymes that participate in uptake and metabolism of non-PTS carbon sources. Unphosphorylated III^{Glc} is an apparent noncompetitive inhibitor of glycerol kinase (GK) with respect to both glycerol and Mg^{2+}–adenosine triphosphate (ATP) (*2*). Inhibition is eliminated upon phosphorylation of III^{Glc} (*2*, *3*). To elucidate the structural basis for the regulatory action of III^{Glc}, we determined the structure of the complex of *E. coli* III^{Glc} with GK and glycerol in the presence and absence of adenosine diphosphate (ADP) by multiple isomorphous replacement, solvent flattening, and crystallographic refinement (Table 1). The model, containing 4991 nonhydrogen atoms, had a conventional crystallographic *R* factor of 0.191 for all data observed between 5 and 2.6 Å resolution. The root-mean-square (rms) deviation was 0.013 Å from ideal bond lengths, 3.1° from bond angles, and 2.3 $Å^2$ from restrained thermal parameters.

GK consists of two large domains, one on either side of a deep and narrow cleft (Figs. 1–3). Regions of the domains that form the cleft are topologically identical to the common ATPase core of hexokinase (*4*), the 70-kD heat shock cognate (HSC70) (*5*), and actin (*6*). We follow the nomenclature established for HSC70. The large domains I and II (Fig. 3A) are divided into smaller subdomains. The two subdomains of the common ATPase fold are denoted IA and IIA. The others, IB, IC, IIB, and IIC, are insertions into or extensions of the common ATPase core (*7*), with IC and IIC unique to GK. Domain IB of GK, consisting of two insertions, is larger than the other IB domains and contains a central five-stranded antiparallel β sheet not found in other members of the family. Although domain IIB is topologically identical to the IIB domains of HSC70 and actin, the tertiary structure of this domain is unrelated to hexokinase, HSC70 or actin.

Glycerol binds at the bottom of the interdomain cleft (Figs. 2A and 3B). The side chains of Arg^{83}, Glu^{84}, Tyr^{135}, and Asp^{245} and the amide NH of Arg^{83} form hydrogen bonds with the hydroxyl groups of glycerol. The side chains of Trp^{103} and Phe^{270} are in van der Waals contact with the carbon backbone of glycerol. Asp^{10} and Asp^{245} form a possible Mg^{2+} binding site. Asp^{10} has been proposed to function in ATP hydrolysis on the basis of its occurrence within a fingerprint sequence derived from the structures of the ATP binding sites of hexokinase, HSC70, and actin (*8*). This fingerprint sequence in GK also led to the prediction that GK would have a fold similar to these three proteins (*8*). Asp^{245} is structurally equivalent to Asp^{211} (*4*, *9*), the putative catalytic base of hexokinase, and is the only amino acid of GK that reacts with affinity labels dibromoacetone and dichloroacetone (*10*). Asp^{245} forms a hydrogen bond with the 3-hydroxyl of glycerol, sug-

J. H. Hurley and H. R. Faber, Institute of Molecular Biology, University of Oregon, Eugene, OR 97403.
D. Worthylake and S. J. Remington, Institute of Molecular Biology and Department of Physics, University of Oregon, Eugene, OR 97403.
N. D. Meadow and S. Roseman, Department of Biology and McCollum-Pratt Institute, The Johns Hopkins University, Baltimore, MD 21218.
D. W. Pettigrew, Department of Biochemistry and Biophysics, Texas A&M University, College Station, TX 77843.

*Present address: Laboratory of Molecular Biology, National Institute of Diabetes, Digestive and Kidney Diseases, National Institutes of Health, Bethesda, MD 20892.
†Present address: Molecular Biology Program, University of Utah, Salt Lake City, UT 84112.
‡To whom correspondence should be addressed.